Nanoscale Research Letters

NANO EXPRESS Open Access

Light Trapping Induced High Short-Circuit Current Density in III-Nitride Nanorods/Si (111) Heterojunction Solar Cells

Ching-Wen Chang[1,2,3], Paritosh V. Wadekar[1], Hui-Chun Huang[4], Quark Yung-Sung Chen[1,5], Yuh-Renn Wu[6], Ray T. Chen[2] and Li-Wei Tu[1,7*]

Abstract

An effective-area photovoltaic efficiency of 1.27% in power conversion, excluding the grid metal contact area and under 1 sun, AM 1.5G conditions, has been obtained for the p-GaN/i-InGaN/n-GaN diode arrays epitaxially grown on (111)-Si. The short-circuit current density is 14.96 mA/cm^2 and the open-circuit voltage is 0.28 V. Enhanced light trapping acquired via multiple reflections within the strain and defect free III-nitride nanorod array structures and the short-wavelength responses boosted by the wide bandgap III-nitride constituents are believed to contribute to the observed enhancements in device performance.

Keywords: III-nitride, Nanorod, Light trapping, Solar cell, Photovoltaic device, Plasma-assisted molecular beam epitaxy

Introduction

The green energy development has become increasingly essential and light-emitting diode (LED) as well as solar cell industries have developed in a fast pace due to an ever-increasing energy crisis. Over the past few decades, III-nitride semiconductors have been successfully applied to LED devices [1–3], which have resulted in substantial commercial benefits. Presently, many scientists seek to exploit the research potential on III-nitrides for photovoltaic applications [4, 5]. Groups III-V nitride materials have many advantages for photovoltaic systems, such as a direct bandgap with a large absorption coefficient [4, 6], a wide bandgap range covering most of the solar spectrum via band engineering [4, 6, 7], high carrier mobility [7], and superior radiation resistance [8]. Based on these superb properties, several device structure designs are simulated, such as InGaN/Si tandem cells [9–14], hot carrier solar cells [15], Schottky-based solar cells [16–18], single [19–24] and multiple [25, 26] junction solar cells, as well as polarization effects on solar cell performance [9, 23, 27]. The simulations have predicted that InGaN/Si heterostructural tandem cells could have efficiencies as high as 21–36% [10, 11, 13] based on different simulation models. The power conversion efficiency (PCE) of InGaN homostructural tandem solar cell with four different In compositions is proposed to be 51% under 1-sun irradiance and 58% under 250-sun concentrated condition [26]. However, the issues of impurities and non-radiative recombination become increasingly significant under low-temperature InGaN thin film growth conditions [28–30]. The significant stacking faults and dislocation densities due to lattice mismatch lead to the decrease in carrier diffusion length and the limitation of solar cell PCE [31–34]. Therefore, numerous challenges remain for the realization of the potential capabilities of high-efficiency III-nitride photovoltaic devices.

In the past decade, many relevant research topics like high-In InGaN crystal growth methods on freestanding

* Correspondence: lwtu@mail.nsysu.edu.tw
[1]Department of Physics and Center of Crystal Research, National Sun Yat-Sen University, Kaohsiung 80424, Taiwan, Republic of China
[7]Department of Medical Laboratory Science and Biotechnology, Kaohsiung Medical University, Kaohsiung 80708, Taiwan, Republic of China
Full list of author information is available at the end of the article

GaN substrate [34], p-type InGaN doping [35], quantum well designs [36–40], electrode designs [41–44], concentrator photovoltaics [37, 41, 45], intermediate band solar cells [46], and reflection-reduced structures [47–49] have been studied. Moreover, the nonpolar nitride-based solar cells were investigated on the polarization effect [50, 51]. Dahal et al. demonstrated a higher than 30%-In InGaN multiple-quantum-well solar cell operation at longer wavelengths (> 420 nm) [38] and illustrated a 3.03% efficiency under increased illumination intensity up to 30 suns [37]. Mori et al. investigated concentrator nitride-based solar cells [45] and addressed the highest PCE of 4% operated at a high light intensity up to 300 suns [41]. Even though several research groups provided different structural or optical designs and improved the growth techniques, the PCE of III-nitride solar cells did not advance much. On the other hand, Reichertz et al. demonstrated that tandem solar cells are feasible by epitaxially growing p-n junction GaN on p-n junction Si substrate [14]. Their results indicated that the Si substrate contributed long-wavelength efficiency while nitride contributed short-wavelength efficiency. Silicon substrates provide not only low-cost solution but also PCE enhancement and good thermal conductivity [52].

Usually, for solar cell growth, continuous film layers are grown on top of each other and this results in high dislocation density. However, when III-nitrides are grown in nanostructures, the bottom area in contact with the substrate is small hence threading dislocations are reduced and strain can also be minimal. Tessarek et al. reported that the dislocations of GaN nanorods vanished as the diameter goes down to 200 nm [53]. Therefore, as an alternative to film growth on silicon substrates, it would be a preferred choice to grow III-nitride nanorod solar cells to reduce the cost, to improve the crystal quality, and to enhance the cell efficiency. Also, nanorod/nanowire has a large capacity for photovoltaic applications because the photo-generated electrons can be collected more effectively before they recombined with holes due to a direct path to the electrodes and nanorod structures can improve light trapping for enhancing photon absorption [54, 55]. Several groups have demonstrated the photodetectors [56, 57], nanolasers [58, 59], nano-LEDs [60, 61], and photoelectrochemical water splitting applications [62] based on III-nitride nanorods [55]. Nonetheless, the demerit of nanorod solar cells is that photo-generated electron-hole pairs recombine at abundant carrier trapping centers due to surface defects. Moreover, the device fabrication processes of nanorod solar cells are more complicated than that of thin film devices. However, overcoming these issues mentioned above has resulted in an almost three-fold increase in PCE as shown by Wallentin et al. where the InP nanorod array has a 13.8% PCE from optimization of the nanorod diameter and the length of the top n-segment [54, 63]. Krogstrup et al. indicated that high short-circuit current density (J_{sc}) was obtained in the single core-shell GaAs nanowire structures due to more than one order of magnitude light absorption enhanced by light concentration [64]. Wierer et al. [65], Cansizoglu et al. [66], and Nguyen et al. [31] demonstrated different types of nitride nanorod-array solar cells on GaN template and Si substrate. The comparison of recent nanorod/nanowire photovoltaic research is listed in Supplementary Information: Table S1. However, the photoelectric conversion contributions of different In content InGaN nanorod ensemble photovoltaic devices on low-cost Si (111) substrates have not been discussed systematically so far.

In this study, Mg:GaN/InGaN/Si:GaN III-nitride nanorod ensembles with 8% and 11% indium concentration were grown on n-doped Si (111) substrates by plasma-assisted molecular beam epitaxy (PA-MBE, Veeco EPI930). The structural properties and indium contents were estimated by high-resolution x-ray diffraction (HR-XRD, Bede D1) measurements. The fine structure of nanorods was analyzed by high-resolution transmission electron microscopy (HR-TEM, FEI E.O Tecnai F20 G2). The current density versus voltage (J-V) properties of nitride solar cells were discussed under 1 sun, AM 1.5G illumination (Newport 94023A). External quantum efficiency (EQE, Enli Technology Co., Ltd., QE-R3018) was measured to study the spectral response. The band diagram alignments and simulations were also investigated to explain the electron and hole transportation.

Experimental Method

Growth Technique

The growth of Si:GaN and Mg:GaN/InGaN/Si:GaN nanorods is based on the plasma-assisted molecular beam epitaxy (PA-MBE) technique. All samples were grown by a Veeco GEN930 PA-MBE system equipped with a 6N nitrogen plasma source (Veeco, UNI-Bulb). The n-type Si (111) substrate with a resistivity of 0.001–0.005 Ω cm was cleaned with acetone, isopropanol, and de-ionized water in an ultrasonic bath for 5 min at each step to remove residual organic contamination and then etched in a 48–51% HF:H_2O = 1:5 solution for 5 min to remove the native oxide. After the chemical cleaning/etching process, the Si substrate was blown dry with nitrogen gas. The Si substrate was introduced into the buffer chamber and then transferred into the growth chamber by a magnetically coupled transfer arm. Prior to the nanorod growth, the substrate was thermally cleaned at 900 °C for 30 min to remove residual native oxide for obtaining a clean and ordered 7 × 7 reconstructed Si surface. The activated nitrogen atoms were generated by a plasma gun and its flux and purity were

controlled via a high-resolution mass flow controller (HORIBA STEC, SEC-7320 M) and a nitrogen purifier (Entegris, CE35KFI4R). The high purity (6N or higher) Ga, In, Si, and Mg sources were provided by solid-source effusion cells. The group III metal and N_2 plasma beam equivalent pressure (BEP) were measured with a beam flux gauge. By controlling the III/V flux ratios to N-rich condition, nanorods can be obtained. First, self-assembled Si:GaN nanorods were grown at 760 °C for 82 min. Desorption of InN is critical at raised temperatures because indium will evaporate from the sample surface. To retain indium in the nanorods, the metal-modulated epitaxy (MME) technique was utilized [67, 68]. MME involves periodic opening and closing of the metal shutters in order to modulate the metal fluxes, while the N_2 shutter is kept open. For tuning In concentration, two different cycle times of In and Ga atoms impinged the substrate alternately for 20 s/30 s (sample B) and 30 s/30 s (sample C) with 50 periods at 550 °C. Finally, Mg:GaN layer was grown at 600 °C. The samples were grown under 9.25×10^{-6} torr active nitrogen BEP with plasma power 450 W, 2.42×10^{-8} torr In BEP, and 1.93×10^{-8} torr Ga BEP. In addition, the single-layer Si:GaN nanorods (sample A) was also prepared as a controlled group under the same condition.

Device Fabrication

After the nanorod growth, the device fabrication process included the following steps. (1) The device area of $350 \times 350\ \mu m^2$ mesa was defined by etching down to the n-type Si with tetrafluoromethane (CF_4) based on the reactive-ion etching technique (Advanced System Technology, Cirie-200) using photoresist (Microchemicals GmbH, AZ1400) as a mask. (2) An ultrasonic bath with de-ionized water was used to clean out loose

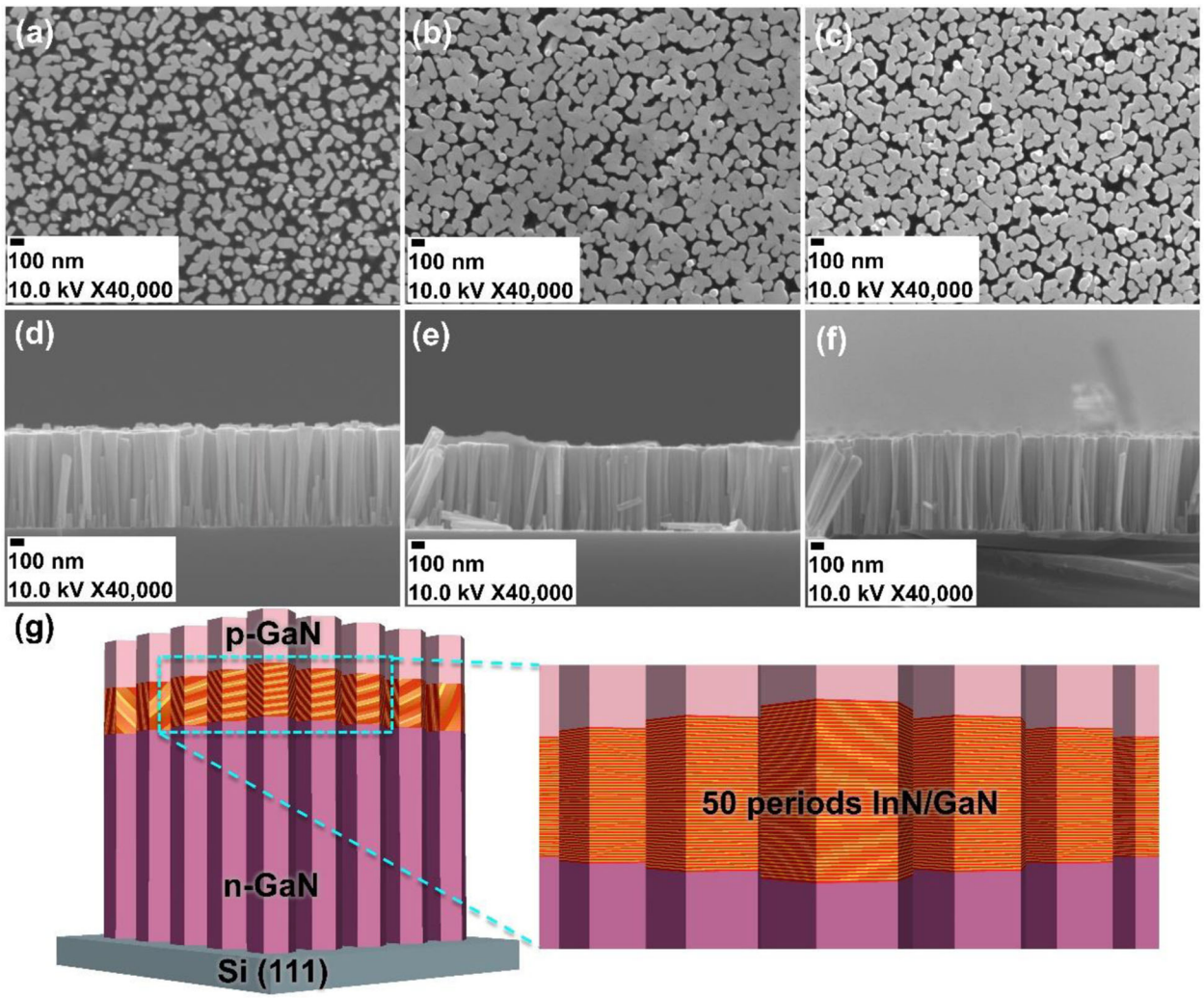

Fig. 1 The SEM top views of **a** n-GaN (sample A), p-GaN/InGaN/n-GaN with the In and Ga atoms impinged cycle times of **b** 20 s/30 s (sample B) and **c** 30 s/30 s (sample C). The SEM cross-section views of **d** sample A, **e** sample B, and **f** sample C. **g** A schematic diagram of p-GaN/InGaN/n-GaN nanorod structure

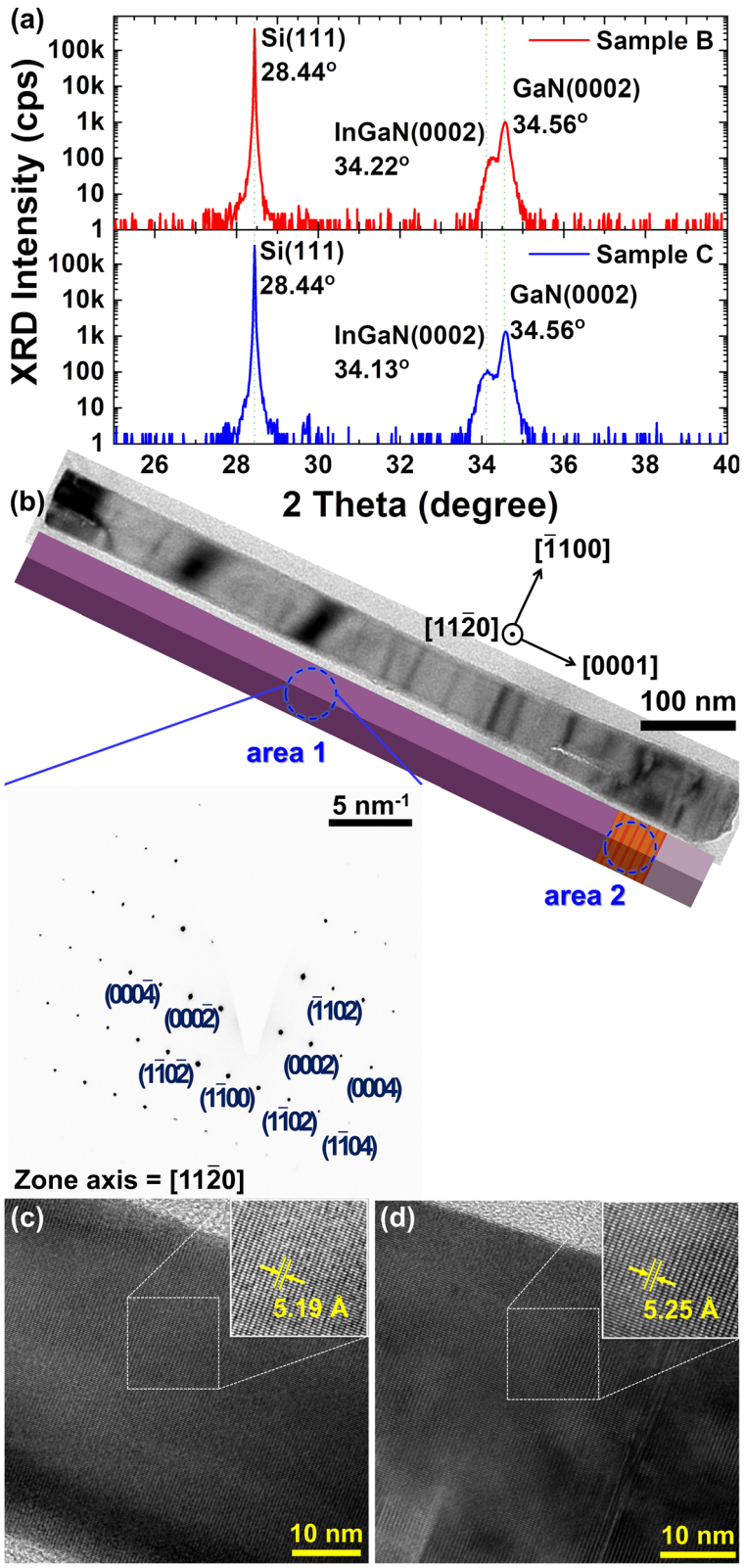

Fig. 2 (See legend on next page.)

(See figure on previous page.)
Fig. 2 a HR-XRD spectra for the theta-2theta scans. The indium content of the InGaN material was estimated to be 8% for sample B (red curve) and 11% for sample C (blue curve) by using Vegard's law. **b** The dislocation-free nitride nanorod TEM image and SAED pattern of n-GaN region. The single nanorod schematic diagram beneath the image obeys the structural relative scale. The atomic-resolution TEM images of **c** n-GaN in area 1 and **d** InGaN in area 2 show dislocation free and their *c* lattice constants

nanorods from the device except those of the mesa area. (3) Immerse the sample in $(NH_4)_2S$ at 60 °C for 1 min to passivate the nitride surface for native oxide suppression and non-radiative recombination reduction [69–73]. (4) A 100-nm indium tin oxide (ITO) thin film was deposited on top of the nanorods to serve as the Mg:GaN ohmic transparent contact by sputtering (Advanced System Technology, Psur-100HB) accompanied by photolithography (M&R Nano Technology, AG350-6B) and lift-off techniques. (5) Multilayer Ti/Al/Ti/Au (20 nm/300 nm/20 nm/50 nm) grid metal contacts on the ITO film and on the n-type Si substrates were fabricated by e-beam evaporation (Advanced System Technology, Peva-600E) using photolithography and lift-off techniques. (6) All grid metal contacts were annealed by rapid thermal annealing system (Advanced System Technology, FA04) for 30 s in nitrogen at 800 °C to obtain ohmic contacts.

TEM Sample Preparation

To further study the crystal structure, individual nanorods of samples B and C were extracted by sonication in ethanol. After 30 min of sonication, a few drops of the ethanol solution were applied to a copper grid (Ted Pella) and the ethanol was evaporated at room temperature. Before the measurements, the sample was baked at 150 °C to remove free organic solvents.

Results and Discussion

Morphological and Structural Properties

The top views and cross-section views of scanning electron microscopy (SEM) images are shown in Fig. 1a–f illustrating the morphology of the as-grown nanorods. From left to right, Fig. 1 a–c represents the variation in the surface morphology of Si:GaN (sample A) and Mg:GaN/InGaN/Si:GaN with varied In/Ga atoms impinging cycle time of 20 s/30 s (sample B) and 30 s/30 s (sample

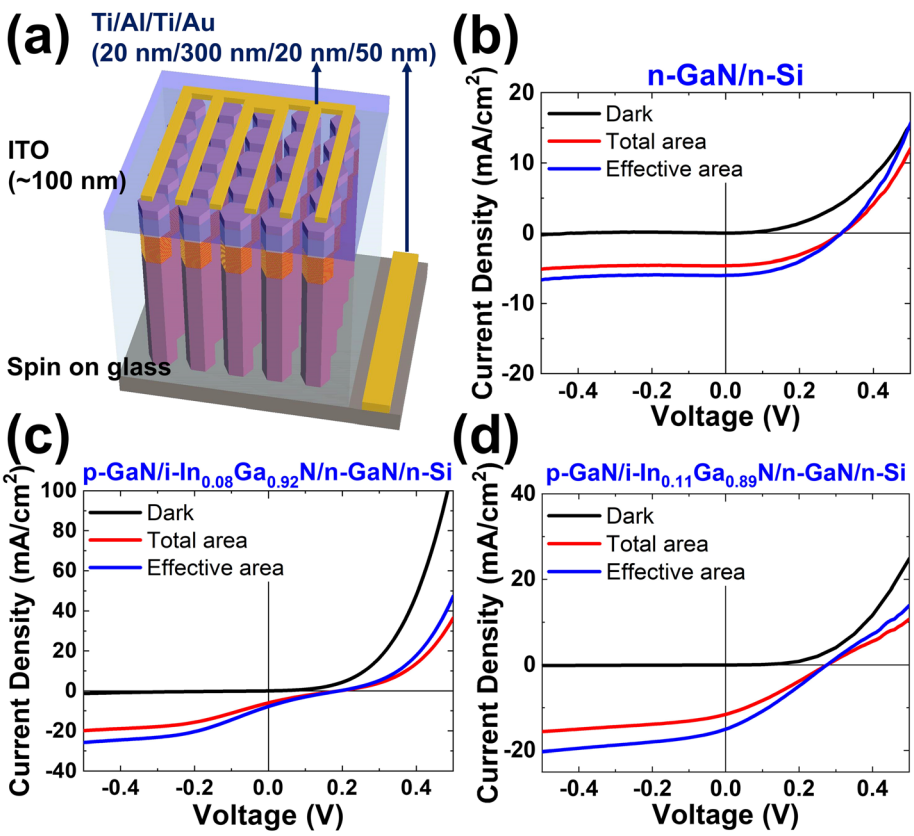

Fig. 3 a The nanorod assemble solar cell schematic diagram. The current density-voltage curves of **b** n-GaN/n-Si, **c** p-GaN/$In_{0.08}Ga_{0.92}$N/n-GaN/n-Si, and **d** p-GaN/$In_{0.11}Ga_{0.89}$N/n-GaN/n-Si nanorod assemble solar cells measured under 1 sun, AM 1.5G solar simulator

Table 1 J_{sc}, V_{oc}, FF, and effective-area PCE comparison of three samples

J_{sc} (mA/cm^2)	V_{oc} (V)	FF (%)	PCE (%)
n-GaN/n-Si (sample A)			
5.98	0.25	35	0.52
p-GaN/i-$In_{0.08}Ga_{0.92}N$/n-GaN/n-Si (sample B)			
7.77	0.19	21	0.31
p-GaN/i-$In_{0.11}Ga_{0.89}N$/n-GaN/n-Si (sample C)			
14.96	0.28	30	1.27

C) during the 50-cycle InGaN growth, respectively. The diameters of Si:GaN and Mg:GaN/InGaN/Si:GaN nanorods are 30–100 nm and 80–150 nm respectively, while the areal densities are ~ 7×10^9 cm^{-2}. The cross-section images of the nanorods are shown in Fig. 1d–f and indicate the length of nanorods to be around 700 nm for samples A to C. The schematic structure of the Mg:GaN/InGaN/Si:GaN samples is shown in Fig. 1g.

Figure 2 a recorded the x-ray theta-2theta diffraction measurement focusing on different source impinging cycle time samples. The strongest peak located at 28.44° originates from the Si substrate. A sharp clear peak at 34.56° corresponds to the GaN (0002) diffraction and indicates good inhibition of phase mixing from the InGaN layer. A peak on the lower 2-theta side of the GaN (0002) peak at 34.22° for sample B and at 34.13° for sample C is InGaN (0002). The *c* lattice constants of InN and GaN are 5.760 Å and 5.185 Å respectively [74]. Following Bragg's law, the *c* lattice constants of InGaN (0002) are calculated as 5.23 Å for sample B and 5.25 Å for sample C. Importing the *c* lattice constant of InGaN (0002) to Vegard's law, the In concentration can be estimated as 8% for sample B and 11% for sample C without

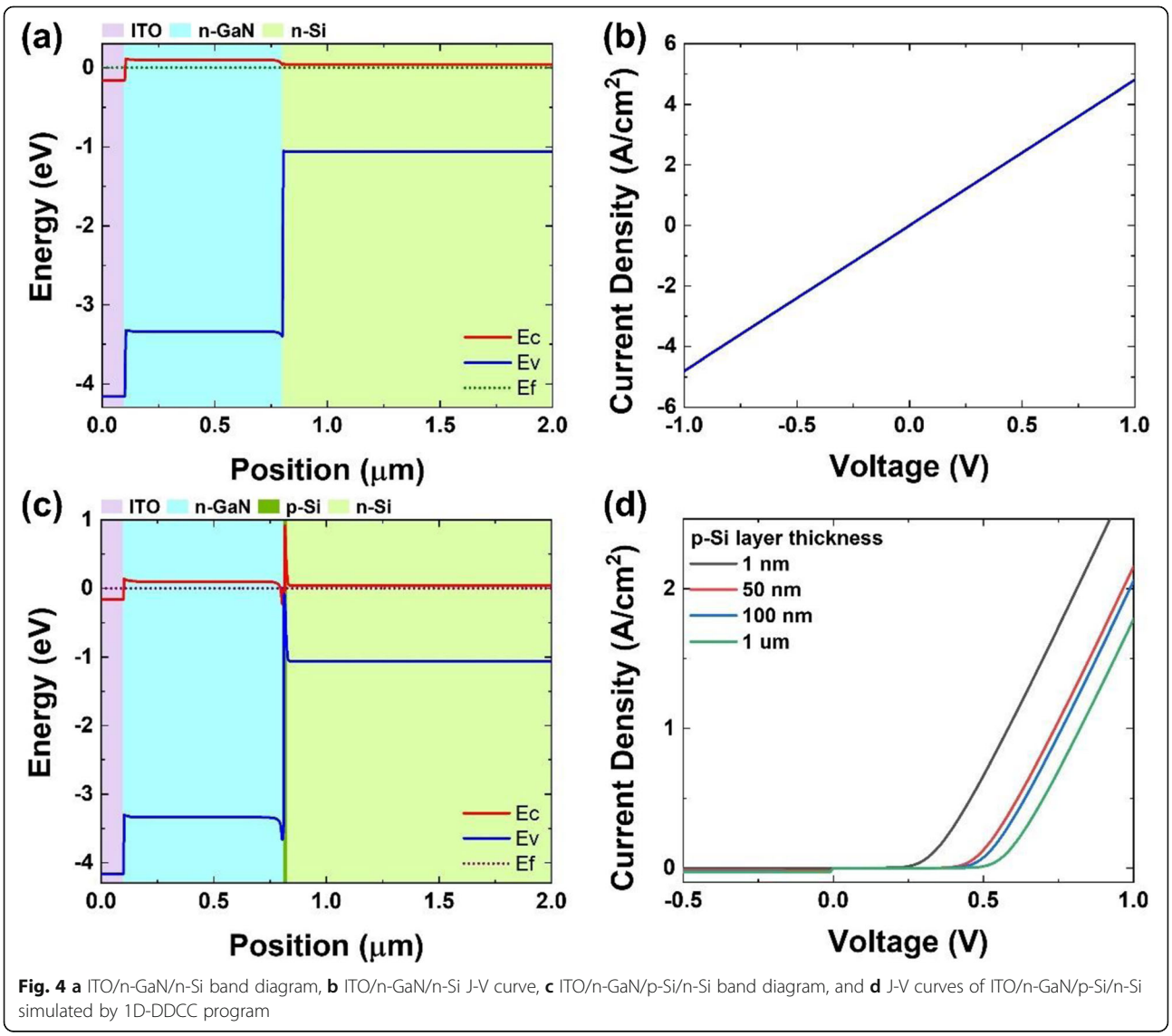

Fig. 4 **a** ITO/n-GaN/n-Si band diagram, **b** ITO/n-GaN/n-Si J-V curve, **c** ITO/n-GaN/p-Si/n-Si band diagram, and **d** J-V curves of ITO/n-GaN/p-Si/n-Si simulated by 1D-DDCC program

consideration of strain. Figure 2 b shows the low magnification TEM image of sample C and schematic diagram of its structure. The area 1 and area 2 are n-GaN and InGaN regions respectively. The selective-area electron diffraction (SAED) pattern taken at the area 1 demonstrates that the [0001] direction is parallel to the long axis of the nanorod and a common growth direction of nitride nanorods. Moreover, no dislocation is found in the crystal. In Figure 2 c and d, the atomic-resolution TEM images yield the *c* lattice constants of GaN and InGaN as 5.19 Å and 5.25 Å respectively, the same as the results calculated by Bragg's law via XRD theta-2theta scan. Moreover, the *c* lattice constant of InGaN for sample B is 5.23 Å via atomic-resolution TEM images shown in the Supplementary Information: Figure S1. In addition, high-angle annular dark-field (HAADF) images and energy dispersive x-ray spectroscopy (EDS) line scan, indicating the indium distribution, are included in Supplementary Information: Figure S2.

Electrical and Optical Characteristics Analysis

The current density versus voltage measurements were performed by a Keithley 2400 source meter. Figure 3 a displays the nanorod assemble solar cell schematic diagram. The total device area is 0.12 mm^2 and the effective area under the illumination excluding the contact metal is 0.0924 mm^2. To collect photon-generated electrons, a 100-nm transparent conductive ITO film is deposited on the top of the p-GaN to connect the nanorods and the Ti/Al/Ti/Au (20 nm/300 nm/20 nm/50 nm) finger electrode. Photoelectric characteristic analyses of the device were also conducted with solar simulator under 1 sun, AM 1.5G condition as shown in Fig. 3b–d. The series resistance R_s values determined from Fig. 3b–d are 83 Ω, 250 Ω, and 2.5 kΩ and the shunt resistance R_{sh} values are 413 kΩ, 550 kΩ, and 2 MΩ for samples A, B, and C respectively. The photocurrent density at zero voltage, J_{sc}, of $In_{0.08}Ga_{0.92}N$ device (sample B) and $In_{0.11}Ga_{0.89}N$ device (sample C) is 7.77 mA/cm^2 and 14.96 mA/cm^2 respectively. The photocurrent enhancement over the increasing In concentration was demonstrated via J_{sc} comparison. Furthermore, Krogstrup et al. illustrated that the light-concentrating property in nanorod solar cells can enhance light absorption and provide high photocurrent [64]. The open-circuit voltage (V_{oc}) and fill factor (FF) of sample C are 0.28 V and 30% respectively. Several groups also demonstrated nanorod structures with lower V_{oc} [72, 75, 76]. To elucidate the real photovoltaic performance in an actually illuminated area, effective-area PCE, PCE_{eff}, establishes an efficiency based on the effective area which excludes the grid electrode area, while total-area PCE, PCE_{tot}, considers the whole device area. It is notable that the PCE_{tot} and PCE_{eff} values are 0.98% and 1.27% which indicate a higher PCE of nitride nanorod solar cell ever reported. The main contribution comes from the high J_{sc}, although the V_{oc} is lower than other III-nitride nanorod solar cell [65, 77]. There are two possible reasons of low V_{oc}, including the quasi-Fermi level limited at the p-n Si junction that Si bandgap is 1.12 eV based on the band diagram and a confined current path may be created due to surface Fermi level pinning [66]. Table 1 summarizes J_{sc}, V_{oc}, FF, and PCE comparison of three samples.

To understand the physical and electrical properties, the band diagrams are calculated by using a 1D-DDCC (One Dimensional Poisson, Drift-Diffusion, and Schrodinger Solver) program [78]. The electron affinities of ITO, Si, and GaN used are 4.40 eV, 4.05 eV, and 4.1 eV

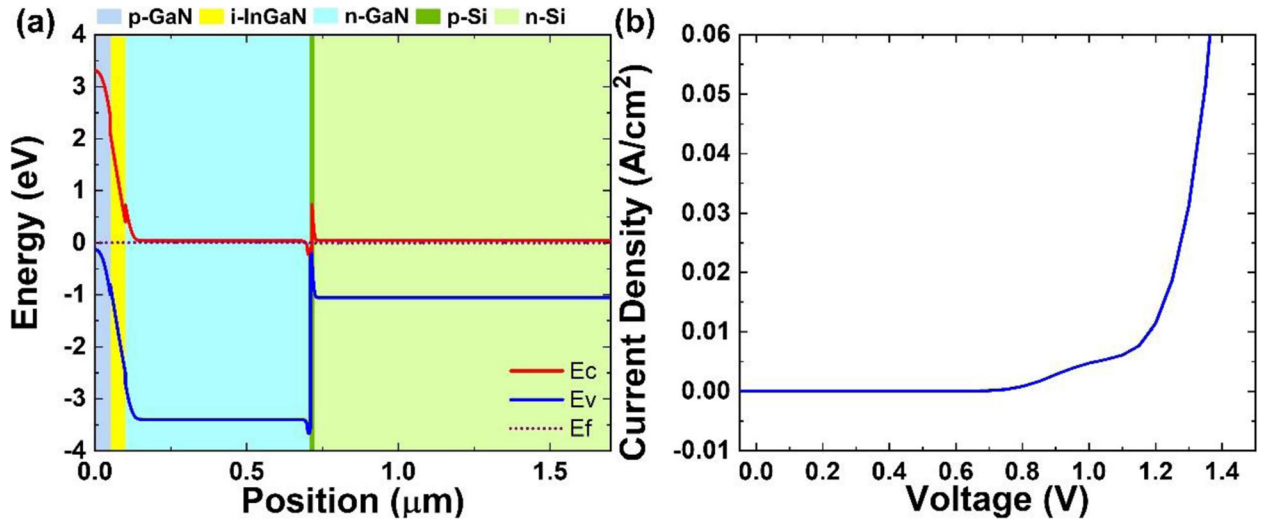

Fig. 5 a The p-i-n nitride nanorod on p-n Si solar cell band diagram simulated by 1D-DDCC program. **b** J-V curve simulation of p-i-n nitride nanorod on p-n Si solar cell

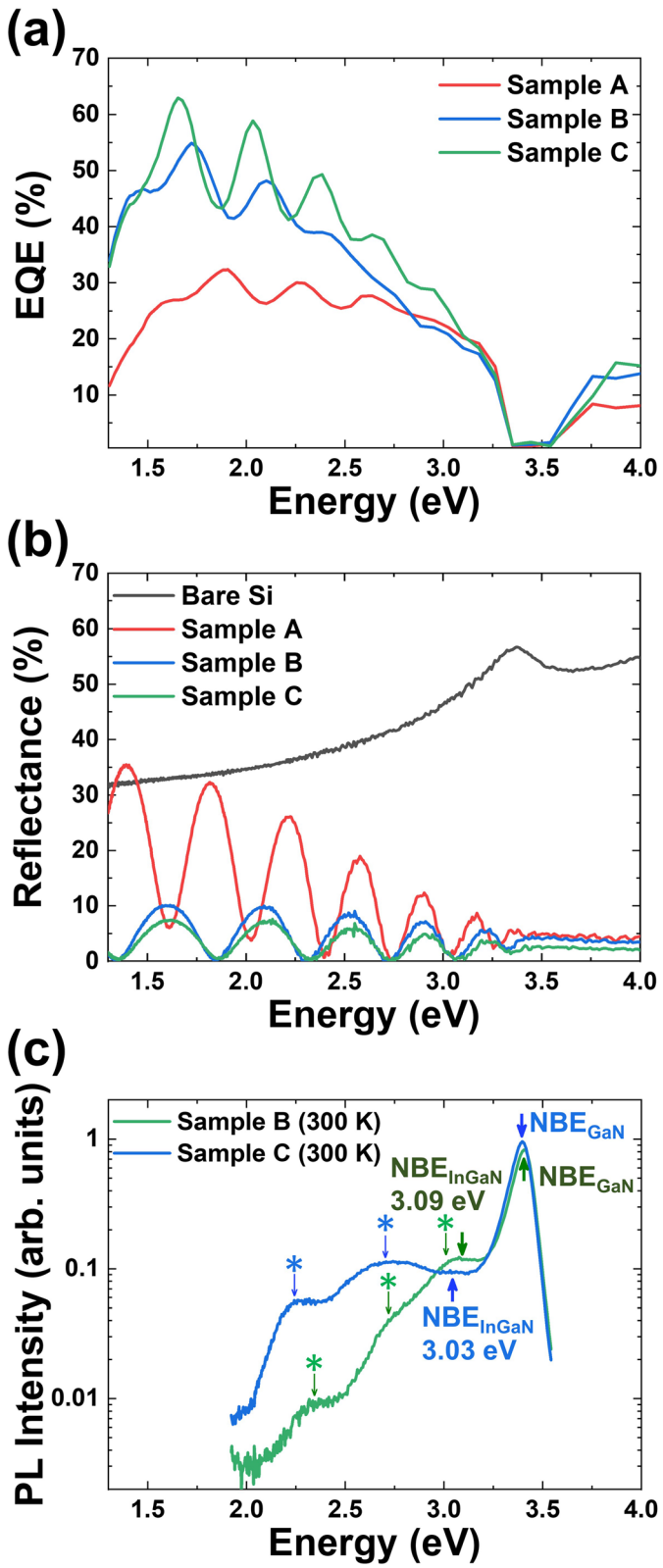

Fig. 6 **a** External quantum efficiency spectra of three nitride nanorods/Si samples. **b** The reflectance spectra of bare Si wafer and three nitride nanorods/Si samples. **c** The room temperature photoluminescence spectra of two InGaN samples

respectively. Figure 4 a and b shows the ITO/n-GaN/n-Si band diagram without voltage bias and J-V curve under dark respectively. It illustrates that the ITO/n-GaN/n-Si structure does not have rectifying effect and shows a linear J-V profile. The potential barrier of the hetero-interface can be ignored for carriers to transport because the conduction band offset between Si and GaN is expected to be a small value of 50 meV. This resistor-like linear J-V curve is in contradiction to the experimental results.

A possible explanation of J-V curve results is that Ga diffusion induces a p-Si at the GaN/Si interface and creates a p-n junction. Reichertz et al. [14] and Neplokh et al. [76] have verified the Al diffusion into the silicon substrate during the growth of nitride layers. Boron, Al, and Ga are IIIB group elements which can be a dopant for p-Si layer formation. However, Ga diffusion rate is 8 nm/day at 700 °C [79]. Figure 4 c shows a band diagram which includes a very thin (1 nm) p-Si layer between n-GaN and n-Si interface. A small built-in electric field is created in p-n Si junction that can drive the electrons to n-Si substrate and holes to ITO contact layer. The thickness-dependent J-V curves demonstrate that the diode turn-on voltage decreases when the thickness of p-Si layers becomes thinner in Fig. 4d. The ultra-thin p-Si will be a limitation for quasi-Fermi level separation and reduce the V_{oc} of solar performance. The simulated electrical property with the p-Si layer included is closer to this research result. Therefore, the band diagram of Mg:GaN/InGaN/Si:GaN/p-Si/n-Si structure can be built as a model as in Fig. 5. Illumination of AM 1.5G light from the top leads to the absorption of photons with energy higher than InGaN bandgap. When light irradiates onto the Si through the rods and the interspace between the rods, the photons with energy larger than Si bandgap could also be absorbed by the p-n Si substrate and photocurrent is produced. Simultaneously, the electron-hole pairs generated in the nitride regions by the short-wavelength light are separated by p-i-n junction built-in electric field. In the end, photo-generated carriers could be collected through the top indium tin oxide (ITO) contact to Mg:GaN and the bottom Si n-contact. Based on this structure model and considering Schottky barrier introduced by ITO contact, the J-V curve simulation is shown in Fig. 5b. The simulated J-V curve indicates that S-shape is caused by non-ohmic behavior of the p-contact. That is a possible reason to explain the S-shape existed for Mg:GaN/u-InGaN/Si:GaN (samples B and C) in Fig. 3 c and d. Therefore, the current densities at negative bias ($J_{\text{negative bias (– 0.5 V)}}$) where the S-shape is flattened are noted in Table S2. $J_{\text{negative bias}}$ can be a checking point for further optimization and a targeted value.

The EQE measurement results without light bias (additional unmodulated light) are shown in Fig. 6a, which compares the EQEs of Si:GaN/n:Si (sample A), Mg:GaN/u-$In_{0.08}Ga_{0.92}N$/Si:GaN (sample B), and Mg:GaN/u-$In_{0.11}Ga_{0.89}N$/Si:GaN (sample C). Sample C has higher In concentration which might be responsible for the higher values at short wavelength due to the absorption in the InGaN layer. The maximum EQEs in samples A, B, and C are 32%, 55%, and 63% respectively. Compared with the reflectance spectra of Si wafer, samples A, B, and C shown in Fig. 6b, the oscillations of EQEs and reflectance spectra are due to the interference from different layers. The bare Si wafer has the highest reflectance due to its flat surface. Samples A, B, and C have lower reflectance because nanorod structures have a light trapping effect. Sample C is found to have the highest EQE at long wavelength and the lowest reflectance due to the highest light trapping effect. This result can explain the higher photocurrent generated in sample C. The room temperature (RT, 300 K) photoluminescence (PL) spectra of sample B and sample C are shown in Fig. 6c. The highest peak located at the 3.40 eV is GaN near band edge (NBE) emission. The peaks located at 3.09 eV and 3.03 eV are due to $In_{0.08}Ga_{0.92}N$ and $In_{0.11}Ga_{0.89}N$ NBE emission. The results are similar to the values from the bowing equation calculation of 3.1 eV and 3.0 eV at RT [4]. It also shows the same strong Fabry-Perot oscillations (marked by star signs) as the EQEs and the reflectance spectra, representing the smooth interfaces between each layer/surface.

Conclusion

High quality Mg:GaN/InGaN/Si:GaN and Si:GaN nanorods grown on n-Si by plasma-assisted molecular beam epitaxy are successfully demonstrated. Photovoltaic measurements exhibit a PCE_{eff} of 1.27% and a PCE_{tot} of 0.98% under 1 sun, AM 1.5G illumination for Mg:GaN/u-$In_{0.11}Ga_{0.89}N$/Si:GaN which has a higher In concentration and a higher light trapping effect inducing a high photocurrent. Although Si:GaN nanorods on n-Si device may not have a prominent p-n junction built-in field, the design of a proper heterojunction structure helps to drive the photocarriers to the top and bottom contacts and enhances the cell performance.

Supplementary information

Supplementary information accompanies this paper at https://doi.org/10.1186/s11671-020-03392-z.

Additional file 1: Table S1. Comparison of the performance of III-nitride nanorods solar cells. **Table S2.** The comparison of photocurrent density at negative biases where the S-shape is flattened. **Figure S1.** The atomic-resolution TEM images of InGaN for $In_{0.08}Ga_{0.92}N$ (Sample B) show dislocation free and lattice constant *c*. **Figure S2.** (a) The HAADF image of Sample C. (b) EDS line scan of a single nanorod.

Abbreviations

LED: Light-emitting diode; PCE: Power conversion efficiency; J_{sc}: Short-circuit current density; PA-MBE: Plasma-assisted molecular beam epitaxy; HR-XRD: High-resolution x-ray diffraction; HR-TEM: High-resolution transmission electron microscopy; EQE: External quantum efficiency; BEP: Beam equivalent pressure; MME: Metal modulated epitaxy; ITO: Indium tin oxide; V_{oc}: Open-circuit voltage; RT: Room temperature; PL: Photoluminescence; NBE: Near band edge

Acknowledgements

The authors gratefully acknowledge the funding supported agencies which are Ministry of Science and Technology, Taiwan and Bureau of Energy, Ministry of Economic Affairs, Taiwan. They also would like to thank Enli Technology Company on the EQE setup and technical discussion.

Authors' Contributions

The idea is conceived by Ching-Wen Chang and Prof. Li-Wei Tu. The most research works were completed by Ching-Wen Chang in National Sun Yat-Sen University under the supervision of Prof. Li-Wei Tu. Prof. Paritosh V. Wadekar and Prof. Quark Yung-Sung Chen are involved in the technical discussion. The manuscript writing was finished in University of Texas at Austin by Ching-Wen Chang under the supervision of Prof. Li-Wei Tu and Prof. Ray T. Chen. TEM fine images were taken by Hui-Chun Huang and analyzed by Ching-Wen Chang. The energy band simulation was done by Ching-Wen Chang under the supervision of Prof. Yuh-Renn Wu. Prof. Li-Wei Tu serves as the principal investigator for the "Wide-Range Hetero-Double Junctions Silicon Solar Cells (NSC 100-3113-E-110-004, NSC 101-3113-E-110-004)" and "Research & Development on Multi-Junction Solar Cell Technology" projects (Bureau of Energy, Ministry of Economic Affairs No. 102-D0606). Prof. Li-Wei Tu and Prof. Ray T. Chen serve as the principal investigators for the "New Partnership Program for the Connection to the Top Labs in the World" (MOST 106-2911-I-110-503) program.

Authors' Information

Dr. CWC, Assistant professor PVW, Dr. HCH, Professor QYC, Professor YRW, Professor RTC, and Professor LWT.

Funding

This study was supported by the Ministry of Science and Technology, Taiwan, ROC (grant No. NSC 100-3113-E-110-004, NSC 101-3113-E-110-004, MOST 106-2911-I-110-503) and Bureau of Energy, Ministry of Economic Affairs, Taiwan, ROC (grant No. 102-D0606).

Availability of Data and Materials

The authors declare that the materials and data are available to the readers, and all conclusions made in this manuscript are based on the data which are all presented and shown in this paper.

Competing Interests

The authors declare that they have no known competing financial interests or personal relationships that could have appeared to influence the work reported in this paper.

Author details

[1]Department of Physics and Center of Crystal Research, National Sun Yat-Sen University, Kaohsiung 80424, Taiwan, Republic of China. [2]Department of Electrical and Computer Engineering, The University of Texas at Austin, Austin, TX 78758, USA. [3]Research Center for Applied Sciences, Academia Sinica, Taipei 11529, Taiwan, Republic of China. [4]Department of Materials and Opto-electronic Science, National Sun Yat-Sen University, Kaohsiung 80424, Taiwan, Republic of China. [5]Department of Physics and Texas Center for Superconductivity, University of Houston, Houston, TX 77004, USA. [6]Institute of Photonics and Optoelectronics and Department of Electrical Engineering, National Taiwan University, Taipei 10617, Taiwan, Republic of China. [7]Department of Medical Laboratory Science and Biotechnology, Kaohsiung Medical University, Kaohsiung 80708, Taiwan, Republic of China.

Received: 16 December 2019 Accepted: 27 July 2020
Published online: 20 August 2020

References

1. Amano H (2015) Growth of GaN on sapphire via low-temperature deposited buffer layer and realization of p-type GaN by Mg doping followed by low-energy electron beam irradiation (Nobel Lecture). Ann. Phys. 527:327–333. https://doi.org/10.1002/andp.201500802
2. Akasaki I (2015) Fascinating journeys into blue light (Nobel Lecture). Ann. Phys. 527:311–326. https://doi.org/10.1002/andp.201500803
3. Nakamura S (2015) Background story of the invention of efficient blue InGaN light emitting diodes (Nobel Lecture). Ann. Phys. 527:335–349. https://doi.org/10.1002/andp.201500801
4. Wu J (2009) When group-III nitrides go infrared: new properties and perspectives. J. Appl. Phys. 106:011101. https://doi.org/10.1063/1.3155798
5. Yamamoto A, Islam MR, Kang TT, Hashimoto A (2010) Recent advances in InN-based solar cells: status and challenges in InGaN and InAlN solar cells. Phys. Status Solidi Curr. Top. Solid State Phys. 7:1309–1316. https://doi.org/10.1002/pssc.200983106
6. Wu J, Walukiewicz W, Yu KM, Ager JW, Haller EE, Lu H, Schaff WJ, Saito Y, Nanishi Y (2002) Unusual properties of the fundamental band gap of InN. Appl. Phys. Lett. 80:3967–3969. https://doi.org/10.1063/1.1482786
7. Walukiewicz W, Ager III JW, Yu KM, Liliental-Weber Z, Wu J, Li SX, Jones RE, Denlinger JD (2006) Structure and electronic properties of InN and In-rich group III-nitride alloys. J Phys D Appl Phys 39:R83–R99. https://doi.org/10.1088/0022-3727/39/5/R01
8. Wu J, Walukiewicz W, Yu KM, Shan W, Ager JW, Haller EE, Lu H, Schaff WJ, Metzger WK, Kurtz S (2003) Superior radiation resistance of $In_{1-x}Ga_xN$ alloys: full-solar-spectrum photovoltaic material system. J. Appl. Phys. 94:6477–6482. https://doi.org/10.1063/1.1618353
9. Lourassi M, Soudini B (2016) Simulation of piezoelectric and spontaneous polarization effect on the InGaN/Si tandem solar cell. Optik. 127:3091–3094. https://doi.org/10.1016/j.ijleo.2015.12.037
10. Hsu L, Walukiewicz W (2008) Modeling of InGaN/Si tandem solar cells. J. Appl. Phys. 104:024507. https://doi.org/10.1063/1.2952031
11. Brown GF, Ager JW, Walukiewicz W, Wu J (2010) Finite element simulations of compositionally graded InGaN solar cells. Sol. Energy Mater. Sol. Cells. 94:478–483. https://doi.org/10.1016/j.solmat.2009.11.010
12. Feng S, Lai C, Tsai CY, Tu LW (2014) Numerical simulations of the current-matching effect and operation mechanisms on the performance of InGaN/Si tandem cells. Nanoscale Res Lett 9:652. https://doi.org/10.1186/1556-276X-9-652
13. El-Huni W, Migan A, Djebbour Z, Salvestrini J-P, Ougazzaden A (2016) High-efficiency indium gallium nitride/Si tandem photovoltaic solar cells modeling using indium gallium nitride semibulk material: monolithic integration versus 4-terminal tandem cells. Prog. Photovoltaics Res. Appl. 24:1436–1447. https://doi.org/10.1002/pip.2807
14. Reichertz LA, Gherasoiu I, Yu KM, Kao VM, Walukiewicz W, Ager JW (2009) Demonstration of a III - nitride/silicon tandem solar cell. Appl. Phys. Express. 2:122202. https://doi.org/10.1143/APEX.2.122202
15. Conibeer G, Shrestha S, Huang S, Patterson R, Xia H, Feng Y, Zhang P, Gupta N, Tayebjee M, Smyth S, Liao Y, Lin S, Wang P, Dai X, Chung S (2015) Hot carrier solar cell absorber prerequisites and candidate material systems. Sol. Energy Mater. Sol. Cells. 135:124–129. https://doi.org/10.1016/j.solmat.2014.11.015
16. Adaine A, Hamady SOS, Fressengeas N (2016) Simulation study of a new InGaN p-layer free Schottky based solar cell. Superlattices Microstruct. 96:121–133. https://doi.org/10.1016/j.spmi.2016.05.020
17. Hamady SOS, Adaine A, Fressengeas N (2016) Numerical simulation of InGaN Schottky solar cell. Mater Sci Semicond Process. 41:219–225. https://doi.org/10.1016/j.mssp.2015.09.001
18. Anderson TH, Lakhtakia A, Monk PB (2018) Optimization of nonhomogeneous indium-gallium-nitride Schottky-barrier thin-film solar cells. J. Photonics Energy. 8:034501. https://doi.org/10.1117/1.JPE.8.034501
19. Wu S, Cheng L, Wang Q (2018) Effects of the unintentional background concentration, indium composition and defect density on the performance of InGaN p-i-n homojunction solar cells. Superlattices Microstruct. 119:9–18. https://doi.org/10.1016/j.spmi.2018.04.033
20. Laref A, Altujar A, Laref S, Luo SJ (2017) Quantum confinement effect on the electronic and optical features of InGaN-based solar cells with InGaN/GaN superlattices as the absorption layers. Sol. Energy. 142:231–242. https://doi.org/10.1016/j.solener.2016.12.009

21. Belghouthi R, Aillerie M, Rached A, Mejri H (2019) Effect of temperature on electronic and electrical behavior of InGaN double hetero-junction p-i-n solar cells. J. Mater. Sci. Mater. Electron. 30:4231–4237. https://doi.org/10.1007/s10854-019-00714-5
22. Fabien CAM, Doolittle WA (2014) Guidelines and limitations for the design of high-efficiency InGaN single-junction solar cells. Sol. Energy Mater. Sol. Cells. 130:354–363. https://doi.org/10.1016/j.solmat.2014.07.018
23. Kazazis SA, Papadomanolaki E, Iliopoulos E (2018) Polarization-engineered InGaN/GaN solar cells: realistic expectations for single heterojunctions. IEEE J. Photovoltaics. 8:118–124. https://doi.org/10.1109/JPHOTOV.2017.2775164
24. Feng SW, Lai CM, Tsai CY, Su YR, Tu LW (2013) Modeling of InGaN p-n junction solar cells. Opt. Mater. Express. 3:1777. https://doi.org/10.1364/ome.3.001777
25. Mesrane A, Mahrane A, Rahmoune F, Oulebsir A (2017) Theoretical study and simulations of an InGaN dual-junction solar cell. J. Electron. Mater. 46: 1458–1465. https://doi.org/10.1007/s11664-016-5176-z
26. Kusakabe K, Yoshikawa A (2014) Proposal for realizing high-efficiency III-nitride semiconductor tandem solar cells with InN/GaN superstructure magic alloys fabricated at raised temperature (SMART). Proc SPIE Gall Nitride Mater Devices IX. 8986:89861B. https://doi.org/10.1117/12.2042121
27. Routray SR, Lenka TR (2017) Spontaneous and piezo-phototronics effect on geometrical shape of III-Nitride wurtzite nanowires for high efficiency photovoltaic applications. Micro Nano Lett. 12:924–927. https://doi.org/10.1049/mnl.2017.0403
28. Koleske DD, Wickenden AE, Henry RL, Twigg ME (2002) Influence of MOVPE growth conditions on carbon and silicon concentrations in GaN. J Cryst Growth. 242:55–69. https://doi.org/10.1016/S0022-0248(02)01348-9
29. Wu XH, Elsass CR, Abare A, MacK M, Keller S, Petroff PM, Denbaars SP, Speck JS, Rosner SJ (1998) Structural origin of V-defects and correlation with localized excitonic centers in InGaN/GaN multiple quantum wells. Appl. Phys. Lett. 72:692–694. https://doi.org/10.1063/1.120844
30. Matioli E, Neufeld C, Iza M, Cruz SC, Al-Heji AA, Chen X, Farrell RM, Keller S, DenBaars S, Mishra U, Nakamura S, Speck J, Weisbuch C (2011) High internal and external quantum efficiency InGaN/GaN solar cells. Appl. Phys. Lett. 98: 021102. https://doi.org/10.1063/1.3540501
31. Nguyen HPT, Chang YL, Shih I, Mi Z (2011) InN p-i-n nanowire solar cells on Si. IEEE J. Sel. Top. Quantum Electron. 17:1062–1069. https://doi.org/10.1109/JSTQE.2010.2082505
32. Movla H, Babazadeh M, Esmaeili SV (2016) A study on the effects of amphoteric defect concentration on the characteristics parameters of $In_xGa_{1-x}N$ thin-film solar cells. Appl. Phys. A Mater. Sci. Process. 122:1–7. https://doi.org/10.1007/s00339-016-0183-8
33. Zhang Y, Kappers MJ, Zhu D, Oehler F, Gao F, Humphreys CJ (2013) The effect of dislocations on the efficiency of InGaN/GaN solar cells. Sol. Energy Mater. Sol. Cells. 117:279–284. https://doi.org/10.1016/j.solmat.2013.06.022
34. Kuwahara Y, Fujii T, Fujiyama Y, Sugiyama T, Iwaya M, Takeuchi T, Kamiyama S, Akasaki I, Amano H (2010) Realization of nitride-based solar cell on freestanding GaN substrate. Appl. Phys. Express. 3:111001. https://doi.org/10.1143/APEX.3.111001
35. Horie M, Sugita K, Hashimoto A, Yamamoto A (2009) MOVPE growth and Mg doping of $In_xGa_{1-x}N$ ($x \sim 0.4$) for solar cell. Sol. Energy Mater. Sol. Cells. 93:1013–1015. https://doi.org/10.1016/j.solmat.2008.11.031
36. Arakawa Y, Ueno K, Noguchi H, Ohta J, Fujioka H (2017) Low-temperature pulsed sputtering growth of InGaN multiple quantum wells for photovoltaic devices. Jpn. J. Appl. Phys. 56:031002. https://doi.org/10.7567/JJAP.56.031002
37. Dahal R, Li J, Aryal K, Lin JY, Jiang HX (2010) InGaN/GaN multiple quantum well concentrator solar cells. Appl. Phys. Lett. 97:30–32. https://doi.org/10.1063/1.3481424
38. Dahal R, Pantha B, Li J, Lin JY, Jiang HX (2009) InGaN/GaN multiple quantum well solar cells with long operating wavelengths. Appl. Phys. Lett. 94:2009–2011. https://doi.org/10.1063/1.3081123
39. Arif M, Elhuni W, Streque J, Sundaram S, Belahsene S, ElGmili Y, Jordan M, Li X, Patriarche G, Slaoui A, Migan A, Abderrahim R, Djebbour Z, Voss PL, Salvestrini JP, Ougazzaden A (2017) Improving InGaN heterojunction solar cells efficiency using a semibulk absorber. Sol. Energy Mater. Sol. Cells. 159: 405–411. https://doi.org/10.1016/j.solmat.2016.09.030
40. Lai KY, Lin GJ, Chen CY, Lai YL, He JH (2011) Origin of hot carriers in InGaN-based quantum-well solar cells. IEEE Electron Device Lett. 32:179–181. https://doi.org/10.1109/LED.2010.2091619
41. Mori M, Kondo S, Yamamoto S, Nakao T, Iwaya M, Takeuchi T, Kamiyama S, Akasaki I, Amano H (2013) Concentrating properties of nitride-based solar cells using different electrodes. Jpn J Appl Phys. 52:08JH02. https://doi.org/10.1117/12.908226
42. Bai J, Athanasiou M, Wang T (2016) Influence of the ITO current spreading layer on efficiencies of InGaN-based solar cells. Sol Energy Mater Sol Cells. 145:226–230. https://doi.org/10.1016/j.solmat.2015.10.026
43. Horng RH, Chu MT, Chen HR, Liao WY, Wu MH, Chen KF, Wuu DS (2010) Improved conversion efficiency of textured InGaN solar cells with interdigitated imbedded electrodes. IEEE Electron Device Lett. 31:585–587. https://doi.org/10.1109/LED.2010.2046615
44. Chang YA, Chen FM, Tsai YL, Chang CW, Chen KJ, Li SR, Lu TC, Kuo HC, Kuo YK, Yu P, Lin CC, Tu LW (2014) Fabrication and characterization of back-side illuminated InGaN/GaN solar cells with periodic via-holes etching and Bragg mirror processes. Opt Express. 22:A1334. https://doi.org/10.1364/OE.22.0A1334
45. Mori M, Yamamoto S, Kuwahara Y, Fujii T, Sugiyama T, Iwaya M, Takeuchi T, Kamiyama S, Akasaki I, Amano H (2012) Concentrating properties of nitride-based solar cells using GaInN/GaInN superlattices. Proc SPIE 8262:82620Z-82620Z–8. https://doi.org/10.1117/12.908226
46. Sheu J, Chen P, Shin C, Lee M, Liao P, Lai W (2016) Manganese-doped AlGaN/GaN heterojunction solar cells with intermediate band absorption. Sol Energy Mater Sol Cells. 157:727–732. https://doi.org/10.1016/j.solmat.2016.07.047
47. Chu MT, Liao WY, Horng RH, Tsai TY, Wu TB, Liu SP, Wu MH, Lin RM (2011) Growth and characterization of p-InGaN/i-InGaN/n-GaN double-heterojunction solar cells on patterned sapphire substrates. IEEE Electron Device Lett. 32:922–924. https://doi.org/10.1109/LED.2011.2144954
48. Han L, French RF, Zhao H (2015) Surface antireflection and light extraction properties of GaN microdomes. IEEE Photonics J. 7:1–9. https://doi.org/10.1109/JPHOT.2015.2403353
49. Yang LM, Pan CY, Lu FP, Chang CW, Feng SW, Tu LW (2015) Anti-reflection sub-wavelength structures design for InGaN-based solar cells performed by the finite-difference-time-domain (FDTD) simulation method. Opt Laser Technol. 67:72–77. https://doi.org/10.1016/j.optlastec.2014.09.016
50. Nakao T, Fujii T, Sugiyama T, Yamamoto S, Iida D, Iwaya M, Takeuchi T, Kamiyama S, Akasaki I, Amano H (2011) Fabrication of nonpolar a-plane nitride-based solar cell on r-plane sapphire substrate. Appl. Phys. Express. 4: 4–6. https://doi.org/10.1143/APEX.4.101001
51. Lai KY, Paskova T, Wheeler VD, Chung TY, Grenko JA, Johnson MAL, Udwary K, Preble EA, Evans KR (2012) Indium incorporation in InGaN/GaN quantum wells grown on m-plane GaN substrate and c-plane sapphire. Phys. Status Solidi Appl. Mater. Sci. 209:559–564. https://doi.org/10.1002/pssa.201127345
52. Liu CY, Lai CC, Liao JH, Cheng LC, Liu HH, Chang CC, Lee GY, Chyi JI, Yeh LK, He JH, Chung TY, Huang LC, Lai KY (2013) Nitride-based concentrator solar cells grown on Si substrates. Sol. Energy Mater. Sol. Cells. 117:54–58. https://doi.org/10.1016/j.solmat.2013.05.017
53. Tessarek C, Bashouti M, Heilmann M, Dieker C, Knoke I, Spiecker E, Christiansen S (2013) Controlling morphology and optical properties of self-catalyzed, mask-free GaN rods and nanorods by metal-organic vapor phase epitaxy. J. Appl. Phys. 114:144304. https://doi.org/10.1063/1.4824290
54. Service RF (2013) Performance of nanowire solar cells on the rise. Science. 339:263–263. https://doi.org/10.1126/science.339.6117.263
55. Zhao S, Nguyen HPT, Kibria MG, Mi Z (2015) III-nitride nanowire optoelectronics. Prog. Quantum Electron. 44:14–68. https://doi.org/10.1016/j.pquantelec.2015.11.001
56. Zhang H, Dai X, Guan N, Messanvi A, Neplokh V, Piazza V, Vallo M, Bougerol C, Julien FH, Babichev A, Cavassilas N, Bescond M, Michelini F, Foldyna M, Gautier E, Durand C, Eymery J, Tchernycheva M (2016) Flexible photodiodes based on nitride core/shell p-n junction nanowires. ACS Appl. Mater. Interfaces. 8:26198–26206. https://doi.org/10.1021/acsami.6b06414
57. DeLuna Bugallo A, Tchernycheva M, Jacopin G, Rigutti L, Julien FH, Chou ST, Lin YT, Tseng PH, Tu LW (2010) Visible-blind photodetector based on p-i-n junction GaN nanowire ensembles. Nanotechnology. 21:315201. https://doi.org/10.1088/0957-4484/21/31/315201
58. Lu YJ, Kim J, Chen HY, Wu C, Dabidian N, Sanders CE, Wang CY, Lu MY, Li BH, Qiu X, Chang WH, Chen LJ, Shvets G, Shih CK, Gwo S (2012) Plasmonic nanolaser using epitaxially grown silver film. Science. 337:450–453. https://doi.org/10.1126/science.1223504
59. Arafin S, Liu X, Mi Z (2013) Review of recent progress of III-nitride nanowire lasers. J. Nanophotonics. 7:074599. https://doi.org/10.1117/1.jnp.7.074599
60. Ra YH, Wang R, Woo SY, Djavid M, Sadaf SM, Lee J, Botton GA, Mi Z (2016) Full-color single nanowire pixels for projection displays. Nano Lett. 16:4608–4615. https://doi.org/10.1021/acs.nanolett.6b01929

61. Jung BO, Bae SY, Lee S, Kim SY, Lee JY, Honda Y, Amano H (2016) Emission characteristics of InGaN/GaN core-shell nanorods embedded in a 3D light-emitting diode. Nanoscale Res. Lett. 11:215. https://doi.org/10.1186/s11671-016-1441-6
62. Chowdhury FA, Mi Z, Kibria MG, Trudeau ML (2015) Group III-nitride nanowire structures for photocatalytic hydrogen evolution under visible light irradiation. APL Mater. 3:0–7. https://doi.org/10.1063/1.4923258
63. Wallentin J, Anttu N, Asoli D, HuffmanM, Åberg I, Magnusson MH, Siefer G, Fuss-Kailuweit P, Dimroth F, Witzigmann B, Xu HQ, Samuelson L, Deppert K, Borgström MT (2013) InP nanowire array solar cells achieving 13.8% efficiency by exceeding the ray optics limit. Science. 339:1057–1060. https://doi.org/10.1126/science.1230969
64. Krogstrup P, Jørgensen HI, Heiss M, Demichel O, Holm JV, Aagesen M, Nygard J, Fontcuberta i Morral A (2013) Single-nanowire solar cells beyond the Shockley-Queisser limit. Nat Photonics. 7:306–310. https://doi.org/10.1038/nphoton.2013.32
65. Wierer JJ, Li Q, Koleske DD, Lee SR, Wang GT (2012) III-nitride coreshell nanowire arrayed solar cells. Nanotechnology. 23:194007. https://doi.org/10.1088/0957-4484/23/19/194007
66. Cansizoglu MF, Hamad SM, Norman DP, Keles F, Badraddin E, Karabacak T, Seo HW (2015) PiN InGaN nanorod solar cells with high short-circuit current. Appl Phys Express. 8:042302. https://doi.org/10.7567/APEX.8.042302
67. Xing Z, Yang W, Yuan Z, Li X, Wu Y, Long J, Jin S, Zhao Y, Liu T, Bian L, Lu S, Luo M (2019) Growth and characterization of high In-content InGaN grown by MBE using metal modulated epitaxy technique (MME). J Cryst Growth. 516:57–62. https://doi.org/10.1016/j.jcrysgro.2019.03.021
68. Moseley M, Gunning B, Lowder J, Doolittle WA, Namkoong G (2013) Structural and electrical characterization of InN, InGaN, and p-InGaN grown by metal-modulated epitaxy. J Vac Sci Technol B Nanotechnol Microelectron Mater Process Meas Phenom. 31:03C104. https://doi.org/10.1116/1.4790865
69. Lin YJ, DaTsai C, Lyu YT, Lee CT (2000) X-ray photoelectron spectroscopy study of $(NH_4)_2S_x$-treated Mg-doped GaN layers. Appl Phys Lett. 77:687–689. https://doi.org/10.1063/1.127086
70. Maruyama T, Yorozu K, Noguchi T, Seki Y, Saito Y, Araki T, Nanishi Y (2003) Surface treatment of GaN and InN using $(NH_4)_2S_x$. Phys Stat Sol C. 0:2031–2034. https://doi.org/10.1002/pssc.200303489
71. Song YM, Kim SH, Kang JH, Park J, Jeon SR, Ryu SW (2013) Surface passivation of high density InGaN/GaN nanorods fabricated by reactive ion etching. J. Nanosci. Nanotechnol. 13:7177–7179. https://doi.org/10.1166/jnn.2013.7696
72. Nguyen HPT, Djavid M, Mi Z (2013) Nonradiative recombination mechanism in phosphor-free GaN-based nanowire white light emitting diodes and the effect of ammonium sulfide surface passivation. ECS Trans. 53:93–100. https://doi.org/10.1149/05302.0093ecst
73. Han SC, Kim JK, Kim JY, Lee DM, Yoon JS, Kim JK, Schubert EF, Lee JM (2013) Ohmic contacts to n-face p-GaN using Ni/Au for the fabrication of polarization inverted light-emitting diodes. J Nanosci Nanotechnol. 13:5715–5718. https://doi.org/10.1166/jnn.2013.7072
74. Morkoç H (2008) Handbook of nitride semiconductors and devices, Wiley-VCH Verlag GmbH & Co. KGaA, Berlin
75. Messanvi A, Zhang H, Neplokh V, Julien FH, Bayle F, Foldyna M, Bougerol C, Gautier E, Babichev A, Durand C, Eymery J, Tchernycheva M (2015) Investigation of photovoltaic properties of single core–shell GaN/InGaN wires. ACS Appl Mater Interfaces. 7:21898–21906. https://doi.org/10.1021/acsami.5b06473
76. Neplokh V, Ali A, Julien FH, Foldyna M, Mukhin I, Cirlin G, Harmand JC, Gogneau N, Tchernycheva M (2016) Electron beam induced current microscopy investigation of GaN nanowire arrays grown on Si substrates. Mater Sci Semicond Process. 55:72–78. https://doi.org/10.1016/j.mssp.2016.03.002
77. Park JH, Nandi R, Sim JK, Um DY, Kang S, Kim JS, Lee CR (2018) A III-nitride nanowire solar cell fabricated using a hybrid coaxial and uniaxial InGaN/GaN multi quantum well nanostructure. RSC Adv. 8:20585–20592. https://doi.org/10.1039/c8ra03127d
78. Wu YR, 1D-DDCC. http://yrwu-wk.ee.ntu.edu.tw/index.php/simulation-program/
79. Kurtz AD, Gravel CL (1958) Diffusion of gallium in silicon. J Appl Phys. 29:1456–1459. https://doi.org/10.1063/1.1722968

Publisher's Note